Chinese Chemical Letters 32 (2021) 1095–1100

Contents lists available at ScienceDirect

Chinese Chemical Letters

journal homepage: www.elsevier.com/locate/cclet

Communication

Selective nitrogen doping on carbon cloth to enhance the performance of zinc anode

Lei Wang, Guilan Fan, Jiuding Liu, Le Zhang, Meng Yu, Zhenhua Yan, Fangyi Cheng*

Key Laboratory of Advanced Energy Materials Chemistry (Ministry of Education), Renewable Energy Conversion and Storage Center, College of Chemistry, Nankai University, Tianjin 300071, China

ARTICLE INFO

Article history:
Received 23 June 2020
Received in revised form 24 July 2020
Accepted 17 August 2020
Available online 18 August 2020

Keywords:
Zinc
Batteries
Nitrogen doping
Carbon substrate
Electrodeposition

ABSTRACT

Metallic zinc is attractive anode material of rechargeable aqueous Zn-based batteries due to its ambient stability, high volumetric capacity, and abundant reserves. Nonetheless, Zn anodes suffer from issues such as low coulombic efficiency (CE), large polarization and dendrite formation. Herein, uniform Zn electrodeposition is reported on carbon substrates by selective nitrogen doping. Combined experimental and theoretical investigations demonstrate that pyrrolic and pyridinic nitrogen doped in carbon play beneficial effect as zinc-philic sites to direct nucleation and growth of metallic Zn, while negligible effect is observed for graphite nitrogen in Zn plating. The carbon cloth with modified amount of doped pyrrolic and pyridinic nitrogen stabilizes Zn plating/stripping with 99.3% CE after 300 cycles and significantly increases the deliverable capacity at high depth of charge and discharge compared to undoped carbon substrate and Zn foil. This work provides a better understanding of heteroatom doping effect in design and preparation of stable 3D carbon-supported zinc anode.

With water as electrolyte solvent, aqueous rechargeable batteries have received increasing attention for the advantages of high ionic conductivity, nonflammability, low toxicity and low cost [1–3]. Metallic zinc serves as a highly promising anode candidate in aqueous zinc-ion batteries (ZIBs) because of its considerable chemical stability in water and air, high volumetric capacity (5855 mAh/cm^3), and globally abundant reserves [4–6]. However, conventional zinc foil anodes suffer from several issues during repeated zinc plating/stripping (Fig. S1a in Supporting information). In alkaline or neutral electrolyte, the passivation caused by the deposition of by-products (*e.g.*, $Zn(OH)_2$ or ZnO) could result in a poor coulombic efficiency and a severe capacity fade [7,8]. Besides, the formation of zinc dendrites may pierce the separator and cause short-circuit [9,10]. Additionally, the parasitic hydrogen evolution causes gassing and self-discharging problems [11–13]. Moreover, as the anode in ZIBs, zinc foil is plagued by either low Zn utilization (at shallow depth of discharge/charge, DOD/DOC) or large shape change (at high depth of discharge/charge) [14,15].

Strategies to address the issues of zinc anode include electrolyte formulation (*e.g.*, high concentrated electrolyte [11,16], gel or solid-state electrolyte [17–19] and electrolyte additives [20–22]), electrode coating or surface modification (*e.g.*, nanoporous $CaCO_3$ coating [23], porous kaolin coating [24]) and 3D architecture design [25,26]. Alternative to the direct use of 2D planar Zn foil, employing 3D substrate to distribute current density is demonstrated to be effective in suppressing dendrite formation and decreasing electrode polarization. Among various 3D substrates, carbonaceous materials such as carbon cloth [27,28] and graphene foam [29] are intriguing freestanding hosts to load metallic zinc because of light weight and high flexibility. Unfortunately, most C atoms in those substrates are tightly bound in a hexagonal lattice with sp^2 hybridization, causing the weak interaction between Zn and substrate, which is unfavored for the nucleation and even growth of metallic Zn. The accessing Zn^{2+} ions are preferred to be attracted by metallic Zn nucleus relative to undeposited carbon substrates due to the lower nucleation overpotential (Fig. S1b in Supporting information). This uneven Zn deposition makes the carbon skeleton underutilized and significantly limits the anodic DOD/DOC. The localized Zn plating/stripping also increases the possibility of dendritic Zn formation [23,30]. Therefore, it is desirable to develop 3D substrates with abundant surface 'zinc-philic' sites for homogenizing Zn deposition.

Heteroatom doping on carbonaceous substrates has been widely adopted in improving the electrode performance [31–33]. Particularly, nitrogen doping could provide not only a

* Corresponding author.
E-mail address: fycheng@nankai.edu.cn (F. Cheng).

https://doi.org/10.1016/j.cclet.2020.08.022
1001-8417/

low energy barrier in the doping reactions, but enhanced interaction between substrates and metal ions, which is demonstrated as an excellent strategy in developing metallic lithium anodes. Nitrogen doping provides abundant lithiophilic sites to enable uniform Li nucleation and growth [34–36]. There are scarce investigations on heteroatom doping of carbon substrates for metallic Zn anode. Recently, 3D N-doped carbon cloth was reported as a favorable host to upgrade both MnO_2 cathode and Zn anode of ZIBs [37]. However, the effect of the N-doped carbon substrate on electrode properties of Zn anode remains not fully understood, as well as the underline mechanism.

In the context of developing advanced Zn anode, herein we present a combined experiment and density function theory (DFT) calculation study on Zn plating/stripping properties of N-doped 3D carbon substrates. The effects of doping concentration and types of nitrogen functional groups (*i.e.*, pyrrolic N, pyridinic N and graphite N) in carbon cloth on the behavior of electrodeposited Zn were comparatively investigated in terms of the morphology change during discharge/charge process, active mass utilization, and cyclability of Zn anode. These results suggest that selective heteroatom doping is promising to improve the electrochemical performances of 3D carbon-supported zinc anode.

Zn@NCC was prepared by hydrothermal treatment of CC followed by a simple electrodeposition method [28], as shown in Fig. S2a (Supporting information). When the pristine CC is used as substrate, undesirable Zn agglomerates are formed *via* the surface diffusion of Zn atoms due to the weak interaction between Zn and CC. The lower nucleation overpotential and stronger Zn-Zn interaction lead to the thermodynamically favorable dendritic deposition in the long running (Fig. S2b in Supporting information). By contrast, when using N-doped CC as substrate, the doped N atoms cannot only provide zinc-philic sites but also enrich the local electron density near the dopant atoms [38–40], which effectively suppresses the Zn aggregation at the initial electrodeposition stage (Fig. S2b in Supporting information). The evenly distributed electron-rich regions on the carbon surface favor the uniform nucleation and following Zn deposition.

N-doped CC samples were prepared by hydrothermal treatment of CC at the temperatures of 120, 150 and 180 °C, which are named as the NCC-1, NCC-2 and NCC-3, respectively. The chemical compositions of N-doped CC samples were studied by FT-IR and EDS analyses. In all three samples, the FT-IR spectra show two peaks at 1230 and 1310 cm^{-1} which can be assigned to the C—N stretching vibrations, and the peaks at 1450 and 1510 cm^{-1} are associated to N—H bending vibrations (Fig. S3a in Supporting information) [41,42]. Elemental mapping in Fig. S3b (Supporting information) reveals that N species are homogeneously distributed on the carbon matrix. The characterization results above have unambiguously proved that the N species are successfully doped on the CC.

To elucidate the state and content of the N in N-doped CC, XPS analysis was conducted and the results are shown in Figs. 1a-c. Three types of nitrogen species could be identified from N 1s spectrum, which can be deconvoluted into pyridinic N (398.5 eV), pyrrolic N (400.1 eV) and graphitic N (402.1 eV), respectively [31,34]. The N contents are determined to be 0.41 at%, 1.21 at% and 1.09 at% for NCC-1, NCC-2 and NCC-3, respectively. From the reported reaction mechanism of N-doping (Fig. S4 in Supporting information) [43], the low nitrogen content of NCC-1 could be attributed to the slow reaction between NH_3 and oxygen-containing functional groups at a low temperature of 120 °C. The slight decrease of N content at 180 °C could be attributed to the

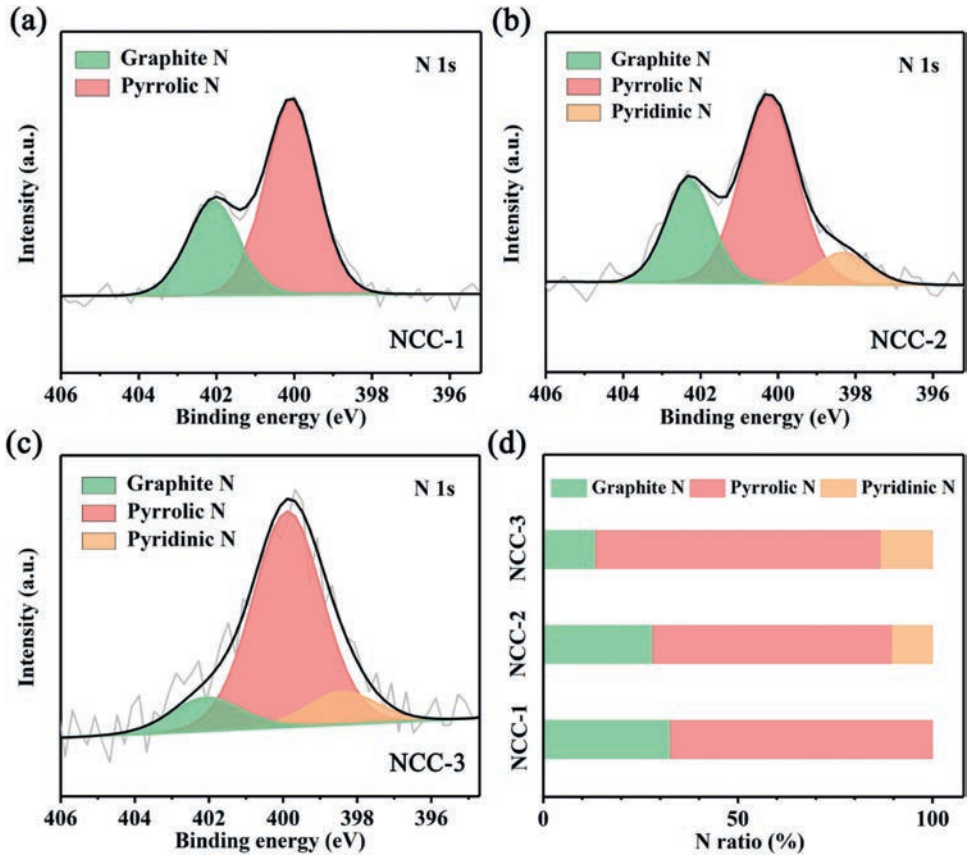

Fig. 1. XPS N 1s spectra of the NCC samples prepared with different hydrothermal reaction temperatures: (a) NCC-1 (120 °C), NCC-2 (150 °C) and NCC-3 (180 °C). (d) The ratios of different nitrogen species in each NCC.

decomposition of reaction intermediates such as amine or amide groups at elevated temperature. Among the three types of nitrogen species, pyrrolic N accounts for the highest proportion in all samples (Fig. 1d). The high fraction of pyrrolic N is attributed to the rich defects and edge sites in low crystallinity carbon material [44].

Considering its highest N content, NCC-2 was first selected as the substrate for Zn electrodeposition. To investigate the effect of the N dopant on Zn deposition, two electrodes of Zn@CC and Zn@NCC were prepared by electroplating metallic Zn on the CC and NCC-2 substrates, respectively. As seen in Fig. S5 (Supporting information), the XRD patterns of both electrodes present intensive peaks at 36.4°, 39.0°, 43.3°, 54.3° and 70.3°, which are consistent with that of the standard metallic Zn, implying a high purity and crystallinity of the deposited Zn. Uneven Zn deposition is one major reason for the instable cycling and irreversible Zn plating/stripping. To comparatively evaluate the performance, two-electrode cells with configurations of Zn foilZn foil, Zn@CCZn@CC and Zn@NCCZn@NCC were assembled and tested electrochemically.

For the Zn foilZn foil cell, the discharge/charge voltage hysteresis is 108 mV at a current density of 0.2 mA/cm^2 and the voltage profile shows irregular fluctuation after 150 h (Fig. 2a). In comparison, the cells based on Zn@CC and Zn@NCC exhibit a much lower polarization with an average overpotential of 44 and 25 mV, respectively. Remarkably, the Zn@NCC displays an excellent cycling stability as evidenced by a negligible voltage fluctuation, and the anode can be further stabilized at ~30 mV for more than 200 h without short circuit. When a higher current density of 1 mA/cm^2 and ending capacity of 0.5 mAh/cm^2 were applied, the Zn@NCC electrode resulted in the lowest polarization (Fig. 2b). The superior electrochemical performance of Zn@NCC to Zn and Zn@CC could be attributed to the 3D structure of carbon substrate with high surface areas to effectively reduce the local current density, and the N dopants to reinforce surface-zinc interaction [39,40].

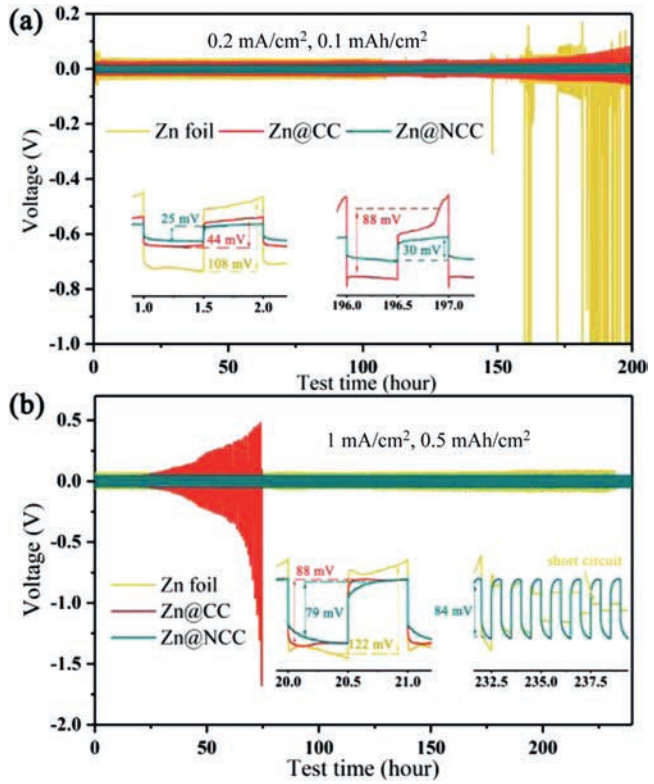

Fig. 2. Galvanostatic discharging-charging profiles of symmetric cells with Zn foil, Zn@CC and Zn@NCC electrodes at the current density of (a) 0.2 mA/cm^2 with ending capacity of 0.1 mAh/cm^2 and (b) 1 mA/cm^2 with the ending capacity of 0.5 mAh/cm^2. Insets enlarge the curves at early and later stage.

To understand the effect of NCC on cycling performance, we studied the morphology evolution of the Zn@NCC electrode at different stages during Zn plating/striping. As shown in Fig. 3a, the Zn surface of foil undergoes protrusion and cracking from the 1st to 150th cycle (Figs. 3a2–a4). Moreover, the Zn foil suffers from exceedingly severe deformation. With the dramatic structure collapse, the average thickness of the foil decreases from 32 μm to 22 μm after 450 cycles (Fig. 3a5), experiencing an electrode thickness change of 31% due to the disordered redistribution of metallic zinc [8,23]. Digital photos of Zn foil and Zn@CC after 450 cycles are shown in Fig. S6 (Supporting information). Compared to Zn@CC, Zn foil shows severer shape change and more disengaged Zn metal on the filter, confirming the superiority of 3D self-supported substrate over traditional Zn foil.

The Zn@CC and Zn@NCC electrodes exhibit an improvement in morphological preservation over Zn foil anode. As shown in Fig. 3b, although Zn slices cover uniformly on the surface of carbon fibers after pre-deposition (Fig. 3b1), they start to fall off after several cycles and the surface of the carbon fibers becomes exposed (Figs. 3b2-b5), which implies an increasingly uneven plating/stripping process. This observation is consistent with the galvanostatic discharging-charging test in Fig. 2. On the contrary, the coating of Zn on Zn@NCC remains intact without filaments, dendrites or uncoated area on the carbon fiber substrate after 450 cycles of Zn plating/stripping (Fig. 3c5). Such comparison supports that the N species are capable of directing uniform Zn deposition/dissolution and suppressing dendrite evolution during continuous cycling. On the other hand, nitrogen dopants improve the electrolyte wettability (Fig. S7 in Supporting information), as can be seen from the lower contact angle of NCC (106.9°) compared to CC (133.2°). The higher electrolyte wettability of NCC benefits the adsorption of Zn^{2+} and uniform nucleation for metallic Zn plating.

Cycling Zn anode in a shallow discharge/charge depth leads to low active mass utilization. Thus, we tested the performance of different electrodes at deep cycling. As shown in Fig. 4a, the initial full discharging Zn foil sustains ~63 h at a current density of 0.127 mA/cm^2. In the following first charge and second discharge stages, the duration significantly declines to 30 and 10 h, respectively. If the DOD is defined as 100%, the corresponding DOC and DORD are 49% and 16%, respectively. A rapid capacity fading from 820 mAh/g to 128 mAh/g is observed for Zn foil (Fig. 4b). Differently, the first specific discharge capacity of Zn@CC (387 mAh/g) is smaller than that of the theoretical value (820 mAh/g), which limits the specific capacity in the following charge (295 mAh/g) and re-discharge processes (221 mAh/g). The corresponding DOD, DOC and DORD of Zn@CC cell are calculated to be 47%, 36% and 16%. The poor performance at deep discharge/charge of Zn@CC could be attributed to the uneven pre-deposition of metallic Zn that causes non-uniform stripping of Zn on deep discharging, as shown in Fig. S8 (Supporting information). Interestingly, the Zn@NCC electrode reaches a high DOD of 95% in first discharging, as a result of the relatively even pre-deposition of Zn for stripping. Furthermore, the Zn@NCC anode could retain higher capacities than Zn foil and Zn@CC in the following charge (430 mAh/g) and discharge stages (380 mAh/g), as shown in Fig. 4b. Thus, the 3D carbon host with nitrogen doping favors uniform Zn deposition for subsequent stripping/plating, mitigating capacity fade of Zn anode at deep charge/discharge.

Previous studies have shown that the N species play a critical role in directing the plating of lithium [34]. However, the effect and mechanism remain unclear in Zn anode. Thus, the electrochemical performances of NCC-1, NCC-2 and NCC-3 were comparatively studied. Fig. 5a shows the voltage profiles. The Zn@NCC-3 cell

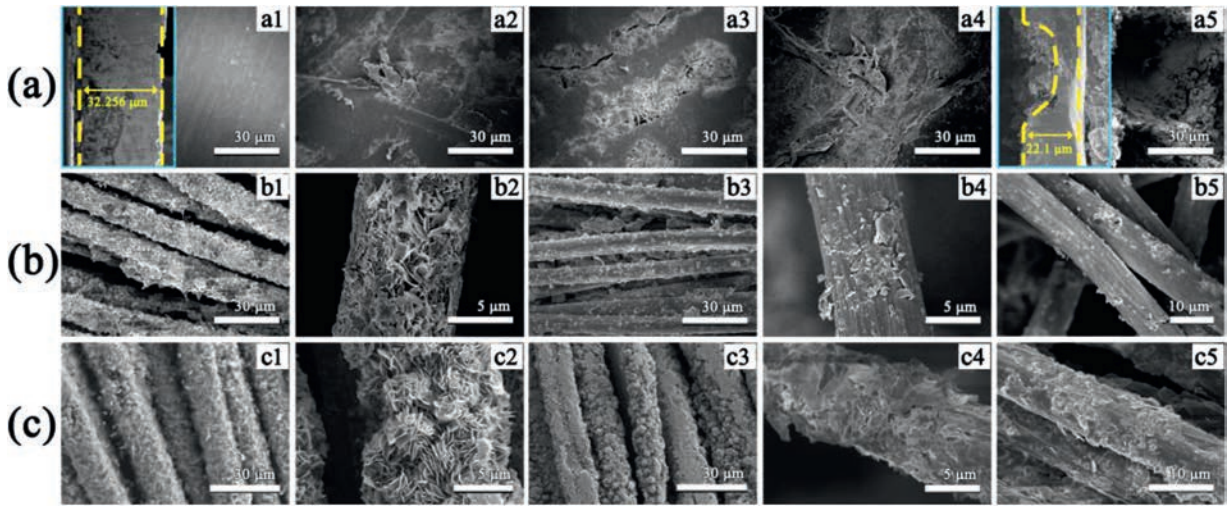

Fig. 3. SEM images of (a) Zn foil, (b) Zn@CC and (c) Zn@NCC during plating/stripping cycles. Numbers 1-5 represent the charge state of the pristine, 1st, 10th, 150th and 450th cycle, respectively. All cells were tested at a current density of 1 mA/cm^2 with the ending capacity of 0.5 mAh/cm^2.

exhibits a low polarization of 87 mV and flat voltage plateaus within 700 cycles at a current density of 1 mA/cm^2. In contrast, there are rapid polarization increases within 600 and 635 cycles for Zn@NCC-1 (from ~90 mV to >200 mV) and Zn@NCC-2 (from ~86 mV to >200 mV), respectively. Besides, coulombic efficiency is a measure of the reversibility of Zn plating/striping of Zn. As seen in Fig. 5b, the NCC-1 and NCC-2 electrodes exhibit average CE values around 80% for 300 cycles and 95% for 200 cycles, respectively, while the average CE of NCC-3 anode maintains 99.3% for 300 cycles. This result suggests a higher reversibility of Zn plating/stripping reaction on NCC-3.

In the case of Li anode, it is believed that pyridinic and pyrrolic nitrogen are the main electrochemically active sites for Li nucleation due to their stronger binding energies with Li atoms than that of graphite nitrogen [34,45,46]. To probe the influence of N species on Zn deposition, the binding energies of Zn with different functional groups were calculated by DFT computations. Herein, the periodic graphene containing 42 carbon atoms with 16 hydrogen atoms terminated at the edges (gra) was modeled [45,47,48]. Additionally, another extended periodic graphene (bgra) was implemented to support the rationality of the constructed model. As shown in Fig. S9 (Supporting information), the difference of the binding energy between gra and bgra with Zn atom is only 0.02 eV, illustrating gra is a reasonable fundamental model for further model specification. The constructed geometry configurations for simulation are shown in Fig. S10 (Supporting information).

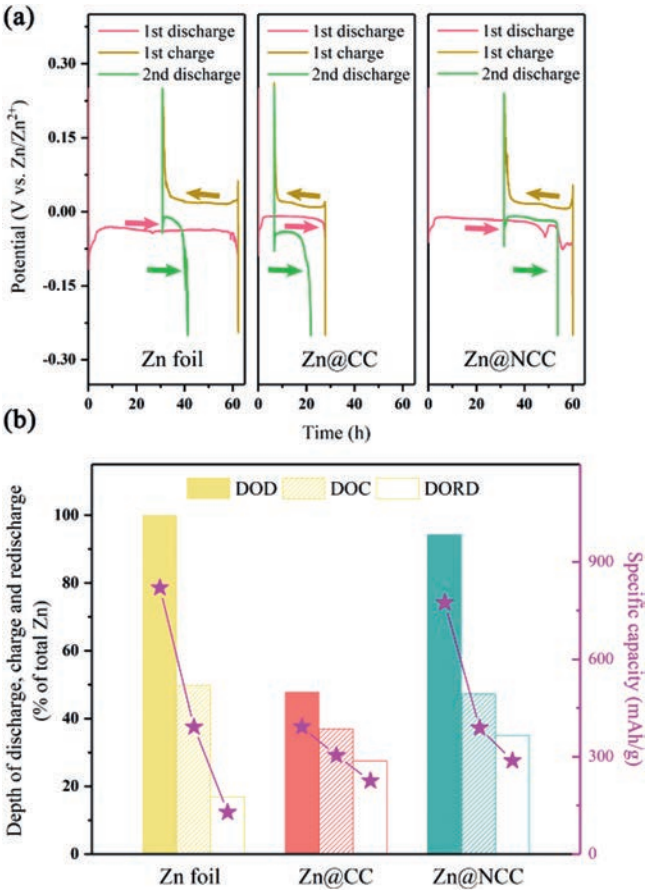

Fig. 4. (a) Total discharge and charge curves of Zn foil, Zn@CC and Zn@NCC in first three processes at the current density of 0.127 mA/cm^2. (b) The corresponding histograms along with the related capacity loss curves of DOD, DOC and DORD.

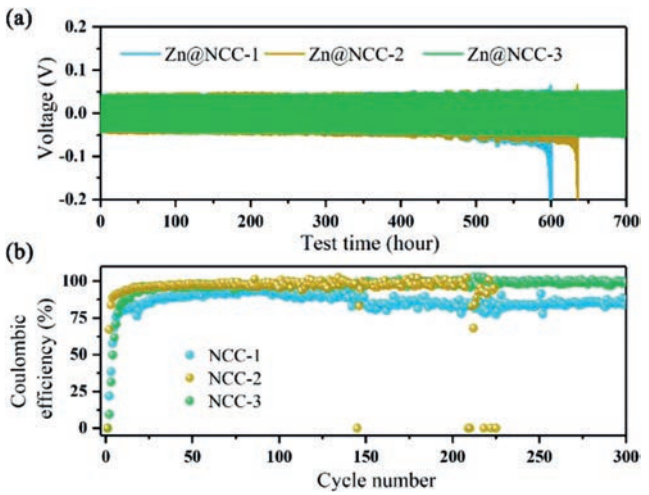

Fig. 5. (a) Galvanostatic discharging-charging profiles of Zn-Zn symmetric cells with Zn@NCC-1, Zn@NCC-2 and Zn@NCC-3 electrodes at the cycling current density of 1 mA/cm^2 with the ending capacity of 0.5 mAh/cm^2. (b) Coulombic efficiencies of asymmetric cells with NCC-1, NCC-2 and NCC-3 electrodes at the current density of 1 mA/cm^2.

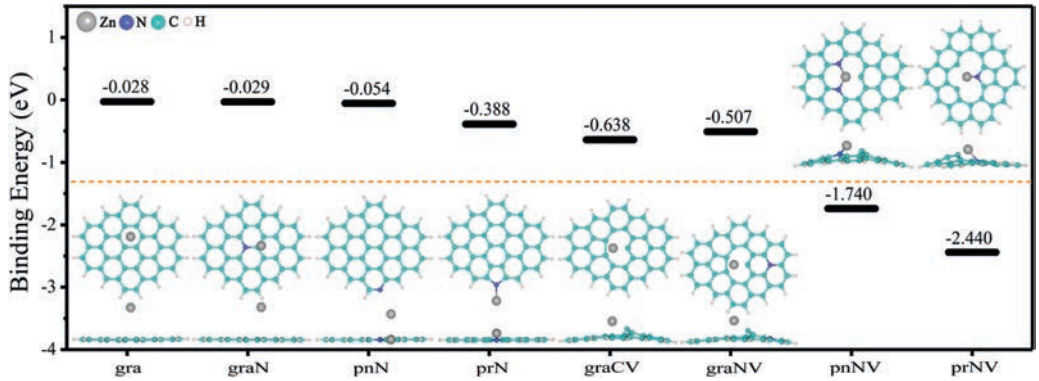

Fig. 6. Summary of calculated binding energy between a Zn atom and pristine or defective graphene substrate with different types of doped nitrogen. Pristine graphene (gra), graphite nitrogen (graN), pyridinic nitrogen (pnN), pyrrolic nitrogen (prN), and their corresponding defective structures graCV, graNV, pnNV, prNV line up on the abscissa axis. The orange dotted line represents the cohesive energy of a Zn dimer in zinc crystal.

Fig. 6 illustrates the optimized binding modes of Zn atoms on perfect/defective graphene with different N species and their binding energies. Other possible geometry configurations are shown in Figs. S11-S17 (Supporting information). The cohesive energy of a Zn dimer is −1.26 eV. A higher binding energy than −1.26 eV suggests prefer formation of Zn clusters, which possibly causes uneven deposition and hence dendrite growth [45,46]. In contrast, a lower binding energy implies a preferential combination of Zn atoms and the matrix, leading to an initially uniform Zn deposition. From the calculated results, prNV and pnNV exhibit lower binding energies of −2.44 and −1.74 eV with Zn atoms than that of graN (−0.029 eV) and graNV (−0.507 eV), indicating strong combination between Zn and pyrrolic/pyridinic N but negligible interaction between Zn and graphite N. Note that the carbon cloth is a kind of graphitic material with low crystallinity and rich defects [44], thus pyrrolic and pyridinic N are more likely to exist as prNV and pnNV in defect condition. The large binding energies of pyrrolic and pyridinic N may be attributed to their extra electrons. The substrate with extra electrons could be regarded as electron-rich donor, which serves as Lewis base sites to adsorb Lewis acidic Zn^{2+} through acid-base interactions [34,36,49] and thus enhances Zn-substrate bonding and directs uniform Zn nucleation. However, the graphite N, both graN and graNV, cannot allow strong adsorption of Zn (Figs. S11 and S15 in Supporting information) because of their saturated electron orbitals. Under this circumstance, Zn atoms are inclined to aggregate, which impedes uniform Zn deposition. Therefore, pyrrolic and pyridinic N play the beneficial roles and serve as zinc-philic sites to stabilize Zn plating/stripping. Thus, the DFT results could explain the superior electrochemical performance of carbon cloth with higher proportion of doped pyrrolic and pyridinic nitrogen.

In summary, uniform Zn deposition was realized by selective nitrogen doping on N-doped carbon cloth and the Zn plating/stripping performance was studied by combining experimental method and DFT computation. Pyrrolic and pyridinic nitrogen are demonstrated as the zinc-philic sites to provide positive effect on homogenizing Zn nucleation and deposition, while graphite nitrogen exerts negligible beneficial effect. The carbon cloth with large proportion of pyrrolic and pyridinic nitrogen stabilizes Zn plating/stripping, delivering a high coulombic efficiency of 99.3% after 300 cycles at a current density of 1.0 mA/cm^2. Compared to Zn foil and undoped carbon substrate, the N-doped carbon cloth with pre-deposited Zn exhibits superior stability for nearly 700 cycles in symmetric cells and significantly mitigates the capacity fading of anode at high depth of charge/discharge. The results indicate the importance of building zinc-philic sites by heteroatom doping carbon substrate and would enlighten the design and preparation of 3D framework-supported zinc anode.

Declaration of competing interest

The authors report no declarations of interest.

Acknowledgments

This work was supported by Tianjin Project (No. 18JCZDJC31100), Ministry of Science and Technology (No. 2017YFA0206702), National Natural Science Foundation of China, (Nos. 21871149 and 21925503), Ministry of Education (No. B12015), and the Fundamental Research Funds for the Central Universities (No. 63201035).

Appendix A. Supplementary data

Supplementary material related to this article can be found, in the online version, at doi:https://doi.org/10.1016/j.cclet.2020.08.022.

References

[1] X. Chen, L. Wang, H. Li, et al., J. Energy Chem. 38 (2019) 20–25.
[2] D. Chao, W. Zhou, C. Ye, et al., Angew. Chem. Int. Ed. 58 (2019) 7823–7828.
[3] L. Su, L. Liu, Y. Wang, et al., Chin. Chem. Lett. 31 (2020) 2358–2364.
[4] F. Wan, X. Wang, S. Bi, et al., Sci. China Chem. 62 (2019) 609–615.
[5] G. Fang, J. Zhou, A. Pan, S. Liang, ACS Energy Lett. 3 (2018) 2480–2501.
[6] D. Xie, F. Hu, X. Yu, et al., Chin. Chem. Lett. 31 (2020) 2268–2274.
[7] K.E.K. Sun, T.K.A. Hoang, T.N.L. Doan, et al., Chem. Eur. J. 24 (2018) 1667–1673.
[8] T.H. Wu, Y. Zhang, Z.D. Althouse, N. Liu, Mater. Today Nano 6 (2019) 100032.
[9] S. Higashi, S.W. Lee, J.S. Lee, et al., Nat. Commun. 7 (2016) 11801.
[10] N. Zhang, F. Cheng, Y. Liu, et al., J. Am. Chem. Soc. 138 (2016) 12894–12901.
[11] F. Wang, O. Borodin, T. Gao, et al., Nat. Mater. 17 (2018) 543–549.
[12] J. Zhang, J. Zhao, H. Du, et al., Electrochim. Acta 280 (2018) 108–113.
[13] Z. Wang, J. Huang, Z. Guo, et al., Joule 3 (2019) 1289–1300.
[14] J.F. Parker, J.S. Ko, D.R. Rolison, J.W. Long, Joule 2 (2018) 2519–2527.
[15] W. Xiong, D. Yang, T.K.A. Hoang, et al., Energy Storage Mater. 15 (2018) 131–138.
[16] X. Wu, Y. Xu, C. Zhang, et al., J. Am. Chem. Soc. 141 (2019) 6338–6344.
[17] Z. Wang, J. Hu, L. Han, et al., Nano Energy 56 (2019) 92–99.
[18] Y. Tang, C. Liu, H. Zhu, et al., Energy Storage Mater. 27 (2020) 109–116.
[19] N. Zhang, X. Chen, M. Yu, et al., Chem. Soc. Rev. 49 (2020) 4203–4219.
[20] K.E.K. Sun, T.K.A. Hoang, T.N.L. Doan, et al., ACS Appl. Mater. Inter. 9 (2017) 9681–9687.
[21] H.A. Bani, G. Kasiri, M.F. La, Electrochim. Acta 258 (2017) 703–708.
[22] M. Huang, S. Huang, S. Chiu, et al., J. Chin. Chem. Soc. 65 (2018) 1239–1244.
[23] L. Kang, M. Cui, F. Jiang, et al., Adv. Energy Mater. 8 (2018) 1801090.
[24] C. Deng, X. Xie, J. Han, et al., Adv. Funct. Mater. 30 (2020) 2000599.
[25] J.F. Parker, C.N. Chervin, I.R. Pala, et al., Science 356 (2017) 415–418.
[26] M. Li, J. Meng, Q. Li, et al., Adv. Funct. Mater. 28 (2018) 1802016.
[27] W. Dong, J. Shi, T. Wang, et al., RSC Adv. 8 (2018) 19157–19163.

[28] Y. Zeng, X. Zhang, Y. Meng, et al., Adv. Mater. 29 (2017) 1700274.
[29] D. Chao, C. Zhu, M. Song, et al., Adv. Mater. 30 (2018) 1803181.
[30] C. Li, S. Liu, C. Shi, et al., Nat. Commun. 10 (2019) 1363.
[31] L. Qie, W. Chen, Z. Wang, et al., Adv. Mater. 24 (2012) 2047–2050.
[32] J. Wang, H. Fan, Y. Shen, et al., Chem. Eng. J. 357 (2019) 376–383.
[33] J. Ma, Z. Xiang, J. Zhang, Sci. China Chem. 61 (2018) 592–597.
[34] R. Zhang, X. Chen, X. Chen, et al., Angew. Chem. Int. Ed. 129 (2017) 7872–7876.
[35] D. Lin, Y. Liu, Z. Liang, et al., Nat. Nanotechnol. 11 (2016) 626–632.
[36] L. Zhao, R. He, K.T. Rim, et al., Science 333 (2011) 999–1003.
[37] W. Qiu, Y. Li, A. You, et al., J. Mater. Chem. A 5 (2017) 14838–14846.
[38] R.B. Sharma, D.J. Late, D.S. Joag, et al., Chem. Phys. Lett. 428 (2006) 102–108.
[39] G.P. Mane, S.N. Talapaneni, C. Anand, et al., Adv. Funct. Mater. 22 (2012) 3596–3604.
[40] J.K. Stark, Y. Ding, P.A. Kohl, J. Electrochem. Soc. 160 (2013) 337–342.
[41] D. Geng, S. Yang, Y. Zhang, et al., Appl. Surf. Sci. 257 (2011) 9193–9198.
[42] S. Huang, Y. Li, Y. Feng, et al., J. Mater. Chem. A 3 (2015) 23095–23105.
[43] L. Sun, L. Wang, C. Tian, et al., RSC Adv. 2 (2012) 4498–4506.
[44] J. Robertson, Adv. Phys. 60 (2011) 87–144.
[45] X. Kong, Q. Chen, Phys. Chem. Chem. Phys. 15 (2013) 12982–12987.
[46] Y. Yang, F. Zheng, G. Xia, et al., J. Mater. Chem. A 3 (2015) 18657–18666.
[47] R.A. Sidik, A.B. Anderson, N.P. Subramanian, et al., J. Phys. Chem. B 110 (2006) 1787–1793.
[48] X. Kong, Z. Sun, M. Chen, et al., Energy Environ. Sci. 6 (2013) 3260–3266.
[49] T. Hou, X. Chen, H. Peng, et al., Small 12 (2016) 3283–3291.